Molecular Diversity
https://doi.org/10.1007/s11030-019-09990-z

ORIGINAL ARTICLE

Design, synthesis, in silico and in vitro evaluation of novel diphenyl ether derivatives as potential antitubercular agents

Ashutosh Prasad Tiwari[1] · B. Sridhar[2] · Helena I. Boshoff[3] · Kriti Arora[3] · G. Gautham Shenoy[1] · K. E. Vandana[4] · G. Varadaraj Bhat[1]

Received: 4 June 2019 / Accepted: 24 August 2019

Abstract

Diphenyl ether derivatives inhibit mycobacterial cell wall synthesis by inhibiting an enzyme, enoyl-acyl carrier protein reductase (InhA), which catalyses the last step in the fatty acid synthesis cycle of genus *Mycobacterium*. To select and validate a protein crystal structure of enoyl-acyl carrier protein reductase of *Mycobacterium tuberculosis* for designing inhibitors using molecular modelling, a cross-docking and correlation study was performed. A series of novel 1-(3-(3-hydroxy-4-phenoxyphenyl)-5-phenyl-4,5-dihydro-1H-pyrazol-1-yl) ethan-1-ones were synthesized from this model and screened for their antitubercular activity against *M. tuberculosis* H37Rv. Compound **PYN-8** showed good antitubercular activity on *M. tuberculosis* H37Rv (MIC = 4–7 µM) and *Mycobacterium bovis* (% inhibition at 10 µM = 95.91%). Cytotoxicity of all the synthesized derivatives was assessed using various cell lines, and they were found to be safe. Structure of **PYN-8** was also confirmed by single-crystal X-ray diffraction. The molecular modelling studies also corroborated the biological activity of the compounds. Further, in silico findings revealed that all these tested compounds exhibited good ADME properties and drug likeness and thus may be considered as potential candidates for further drug development.

Graphic abstract

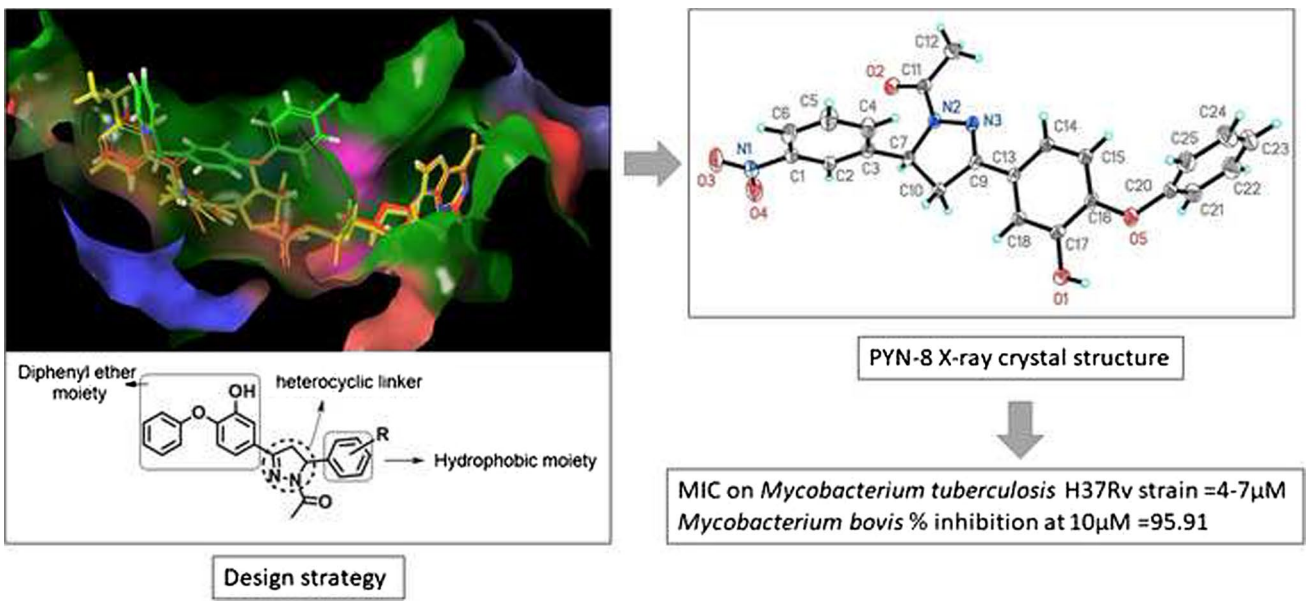

Electronic supplementary material The online version of this article (https://doi.org/10.1007/s11030-019-09990-z) contains supplementary material, which is available to authorized users.

Extended author information available on the last page of the article

Published online: 10 September 2019

Keywords TB · Diphenylether · InhA · Molecular docking · Correlation study · Antitubercular

Introduction

Tuberculosis (TB) is the major cause of death from a single infectious agent (above HIV/AIDS). It is also one among leading 10 causes of death [1]. About 1.3 million deaths among HIV-negative and an additional 0.3 million in HIV-positive people in 2017 were due to TB. Though this indicates the overall results of all countries and age groups, 90% of them were adults (age ≥ 15 years), in the most productive years of their life. Millions of deaths are prevented each year, about 54 million in 2000–2017, with timely diagnosis and treatment [2]. The success rates of treatment for the new cases are around 82% globally, as indicated by latest data of the treatment outcome in 2016. TB treatments take too long to cure and can be toxic. They are also complicated to administer which results in poor patient compliance [3]. New treatments that are faster, simpler and affordable are urgently needed.

A validated target for *Mycobacterium* is enoyl-acyl carrier protein reductase (InhA) [4]. It is an enzyme in the type II fatty acid synthase system, contributing to the biosynthesis of mycolic acids. Mycolic acids are a chief component of mycobacterial cell wall and are responsible for virulence of the microorganism [5]. InhA catalyses the reduction of the double bond of 2-trans-enoyl-[acyl carrier protein] in a NADH-dependent manner, which is the last and a crucial step of the FAS-II pathway, involved in the fatty acid elongation cycle. Isoniazid (INH), a first line antitubercular drug, targets this enzyme. InhA is inhibited by an active form of isoniazid which is formed by reacting with the cofactor NAD(H), bound to the active site of the enzyme. It forms a covalent adduct (isonicotinic acyl NADH), which binds to InhA with high affinity [6]. The activation is carried out by the catalase peroxidase enzyme encoded by *katG*, and mutation in this gene is the cause of resistance to isoniazid in 64% of clinical isolates [7]. Therefore, molecules which directly inhibit InhA without any bio-activation circumvent this mechanism of resistance and are promising candidates. Such a direct inhibitor of InhA is triclosan (a diphenyl ether derivative) [8]. However, it is a weak inhibitor of InhA [9]. Therefore, in the present work, a series of diphenyl ether derivatives were designed and synthesized by studying the nature of the substrate binding pocket and the interactions of potent

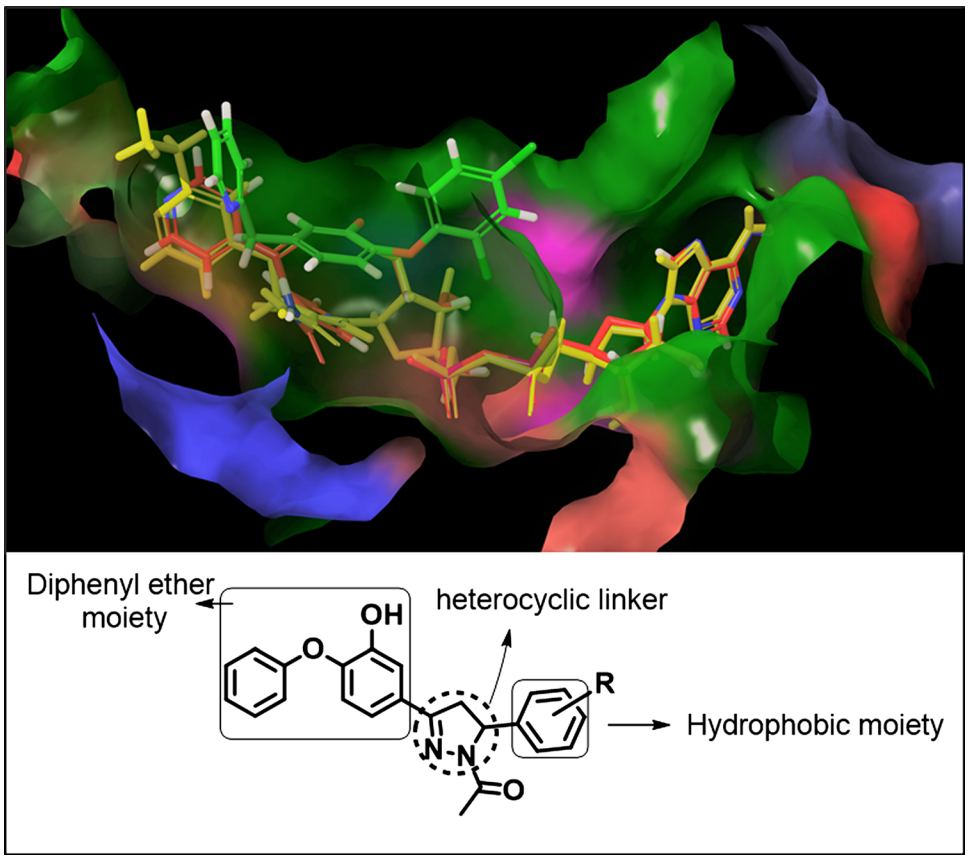

Fig. 1 Design strategy and active site of InhA showing diphenyl ether derivative substituted at 5th chlorine position protruding into the isonicotinoyl binding pocket containing InhA complexes of isoniazid (red colour) and ethionamide (yellow colour). (Color figure online)

Table 1 RMSD of the extracted ligands after docking on the respective crystal structures with poses in their native crystal structure

Co-crystallized ligand	2X23	4OYR	4OXY	4OXK	4OHU	2X22	3FNH	3FNG	3FNF	3FNE	1P45	Average RMSD (Å)	Outliers
Protein crystal structure													
2X23 with water	0.893	0.955	0.631	1.164	1.118	0.301	10.313	2.043	1.784	1.591	1.004	**1.982**	**2**
2X23 without water	0.849	0.954	0.595	1.637	1.09	0.921	10.443	1.382	1.785	1.589	1.001	**2.022**	**1**
4OYR with water	1.393	0.254	1.516	10.689	1.298	1.365	10.415	2.2	1.941	1.715	9.422	**3.837**	**4**
4OYR without water	1.391	0.226	0.817	2.011	1.336	1.363	1.979	8.909	1.941	1.715	10.116	**2.891**	**3**
4OXY with water	1.192	1.334	1.237	1.985	1.512	1.111	2.028	2.021	1.725	1.678	0.76	**1.508**	**2**
4OXY without water	1.166	1.066	1.08	2.362	1.367	1.069	2.125	1.212	1.059	1.696	0.726	**1.357**	**2**
4OXK with water	0.97	1.195	1.232	1.324	1.401	1.151	1.79	1.891	0.622	0.637	0.599	**1.165**	**0**
4OXK without water	0.971	0.778	1.232	1.328	1.453	1.169	1.739	0.985	0.75	0.713	0.649	**1.070**	**0**
4OHU with water	1.72	0.847	1.109	11.336	0.452	1.669	9.724	2.181	9.467	8.857	6.168	**4.866**	**6**
4OHU without water	1.046	0.866	1.108	11.757	0.306	1.009	9.723	2.186	9.197	8.857	6.168	**4.748**	**6**
2X22 with water	0.893	1.271	0.629	9.51	1.306	0.848	9.866	8.854	8.816	9.038	9.091	**5.466**	**6**
2X22 without water	1.011	0.959	0.984	11	1.308	0.896	9.872	8.851	8.828	9.054	8.988	**5.614**	**6**
3FNH with water	2.321	1.703	1.709	1.428	2.398	2.375	1.667	1.645	0.663	1.318	0.571	1.618	3
3FNH without water	2.321	1.703	1.709	1.428	2.398	2.375	1.667	1.645	0.663	1.318	0.571	**1.618**	**3**
3FNG with water	1.179	1.435	1.178	1.427	1.648	1.262	1.451	1.744	0.611	0.534	0.592	**1.187**	**0**
3FNG without water	1.273	1.483	0.918	1.209	1.705	1.345	1.481	1.735	0.515	1.911	0.591	**1.288**	**0**
3FNF with water	1.128	1.582	1.144	1.164	1.789	1.272	1.91	0.737	0.763	0.943	0.486	**1.174**	**0**
3FNF without water	1.411	1.538	1.51	1.452	1.835	1.557	2.233	0.672	0.713	0.706	0.659	**1.299**	**0**
3FNE with water	1.126	1.197	1.292	1.501	1.325	1.183	1.095	0.962	0.608	0.302	0.442	**1.003**	**0**
3FNE without water	1.549	1.239	1.045	1.445	1.315	1.647	1.604	0.508	0.351	0.298	0.45	1.041	**0**
1P45 with water	2.001	1.356	1.643	1.987	1.512	2.04	2.178	1.879	0.839	1.576	0.572	**1.598**	**3**
1P45 without water	1.207	1.369	1.641	2.248	1.418	1.214	2.331	0.697	0.839	1.592	0.609	**1.379**	**2**

inhibitors with the amino acid residues of the active site. The design used in this work is shown in Fig. 1.

Physicochemical properties of the inhibitor molecules are a major factor for drug efficacy. Therefore, Lipinski's rule was followed while designing the molecules to fulfil these requirements. The synthesized compounds were screened against H37Rv strain of *Mycobacterium tuberculosis* and *Mycobacterium bovis*. The safety profiles of the molecules were also determined using various cell lines. To study the plausible mechanism of inhibition and for determination of ADME profile of the synthesized molecules, molecular modelling study was carried out.

Results and discussion

Protein crystal structure selection

To select and validate a protein crystal structure of enoyl-acyl carrier protein reductase of *Mycobacterium tuberculosis* for designing of the inhibitor molecules using molecular modelling, a cross-docking and correlation study was performed. There are 87 crystal structures available hitherto in the protein data bank for the protein, enoyl-acyl carrier protein reductase, of *Mycobacterium tuberculosis* of strain H37Rv. It was thus essential to select a right protein crystal structure, for the design and docking studies of the inhibitor molecules. The primary prerequisite for selection of the protein crystal structure is the presence of a co-crystallized ligand in it, which is similar to the inhibitor molecule scaffold. The protein crystal structure should be able to accommodate all the analogues of the scaffold molecule without much deviation, so as to corroborate the in vitro activity results. Thus, a cross-docking study involving docking of the co-crystallized ligands extracted from the selected protein crystal structures on each of the protein crystal structures was performed. The protein crystal structures were selected based on screening parameters mentioned in the experimental section.

Cross-docking study

All the ligands extracted from the 11 proteins were docked on every protein. Root-mean-square deviation (RMSD) of every ligand with its docked pose in all the proteins, relative to its pose in the aligned ligand set, was calculated. The

values of the RMSDs are listed in Table 1. Ligands with RMSD values more than 2 Å were considered as outliers. The protein crystal with the least number of outliers and the least average RMSD value was thought to be appropriate for use to study the docking of a variety of diphenyl ether derivatives. The protein with PDB entry code 3FNE had the least average RMSD value and no outliers. It had a resolution of 1.98 Å and a triclosan derivative, 2-(2,4-dichlorophenoxy)-5-(pyridin-2-ylmethyl) phenol as its co-crystallized ligand.

Correlation study

To validate the outcome of the cross-docking study and therefore the applicability of the protein 3FNE, a correlation study was done. Twenty-five molecules from the literature with their experimental IC_{50} values were collected [10–12]. These molecules were then docked on the protein 3FNE. Molecular mechanics/generalized born surface area (MM/GBSA) was used to calculate the binding free energy of the ligand–protein complex. Prime MM/GBSA calculations were performed for the complexes obtained after docking of the molecules on 3FNE, and the pIC_{50} values were correlated with the free binding energy of the ligand–protein complexes. The MM/GBSA values and the pIC_{50} values as listed in Table 2. A graph was plotted between the MM/GBSA values and the pIC_{50} values, and a Pearson's correlation coefficient value of 0.73 was obtained (Fig. 2). This validates the protein crystal structure 3FNE chosen after the screening of the available crystal structures of InhA. It also hints that the mechanism of action of the synthesized diphenyl ether derivatives could plausibly be the inhibition of InhA.

Drug design strategy

Molecules were designed by studying the nature of the substrate binding pocket of InhA. Also, the interactions of various potent direct inhibitors (diphenyl ether analogues) with the amino acid residues, as exhibited in their protein crystallographic structures, were studied. Sullivan et al. reported the crystal structures of diphenyl ether derivatives complexed with InhA, giving detailed insight into the binding pocket interactions with the direct inhibitors. A basic scaffold was then assigned which had the attributes required for interactions in a favourable way with the binding pocket. Hydrogen bonding interaction between amino acid residue tyrosine 158 and the hydroxyl group of the diphenyl moiety was considered essential for activity [13]. Also, the π–π stacking interaction of the phenyl ring of the diphenyl ether moiety with the pyridyl moiety of the NAD 300 cofactor InhA protein was observed in potent inhibitors [14]. Comparison of the crystal structures of InhA complexes of isoniazid-NAD and ethionamide-NAD adducts with InhA–triclosan complex gives clues for structural modifications in diphenyl ether scaffold for increasing affinity towards InhA [15]. Hydrophobic substitutions in place of the chloro group at 5 position of A ring in diphenyl ether scaffold might help in occupying and increasing interactions with isonicotinoyl binding pocket which is important for improved activity [16]. Additionally for the better positioning of the aryl group (hydrophobic substituent) into the target INH binding pocket, a heterocyclic linker was designed between the hydrophobic moiety and the 5th carbon position on A ring.

Table 2 Binding free energy of diphenyl ether analogues (with respective codes as in the reference) from the literature with their IC_{50} and pIC_{50} values

Molecules	IC_{50}	pIC_{50}	ΔG Bind (Kcal/mol)
8PP	5	8.30103	−90.4033
PT092	10	8	−91.3701
PT113	12.1	7.917215	−86.8914
5PP	17	7.769551	−82.6221
PT095	29.7	7.527244	−82.4981
PT096	44.6	7.350665	−86.2859
PT114	48	7.318759	−90.9673
13b	48	7.318759	−86.7372
PT070	50.7	7.294992	−90.5046
14c	55	7.259637	−88.0505
PT013	61.9	7.208309	−88.3477
PT133	79.7	7.098542	−86.73
4PP	80	7.09691	−80.3218
PT109	86	7.065502	−83.2069
PT111	100	7	−87.3732
14PP	150	6.823909	−73.6168
3b	236	6.627088	−80.5168
PT134	238.8	6.621966	−80.0489
3e	650	6.187087	−81.2368
10a	1550	5.809668	−67.8625
PT108	1570	5.8041	−77.4535
2PP	2000	5.69897	−71.675
11a	2360	5.627088	−58.3266
12a	3200	5.49485	−64.9083
2d	100,000	4	−62.3432

Induced fit docking

Induced fit docking (IFD) of the synthesized PYN-8 and triclosan generated good poses with RMSD of 0.093 Å. PYN-8 showed hydrogen bonding interaction indicated by yellow dotted lines, with the tyrosine 158 residue. A π–π stacking interaction with the pyridyl ring of NAD 300 was observed (indicated by blue dotted line). A cation–π interaction (indicated by green dotted line) with the pyridine nitrogen of

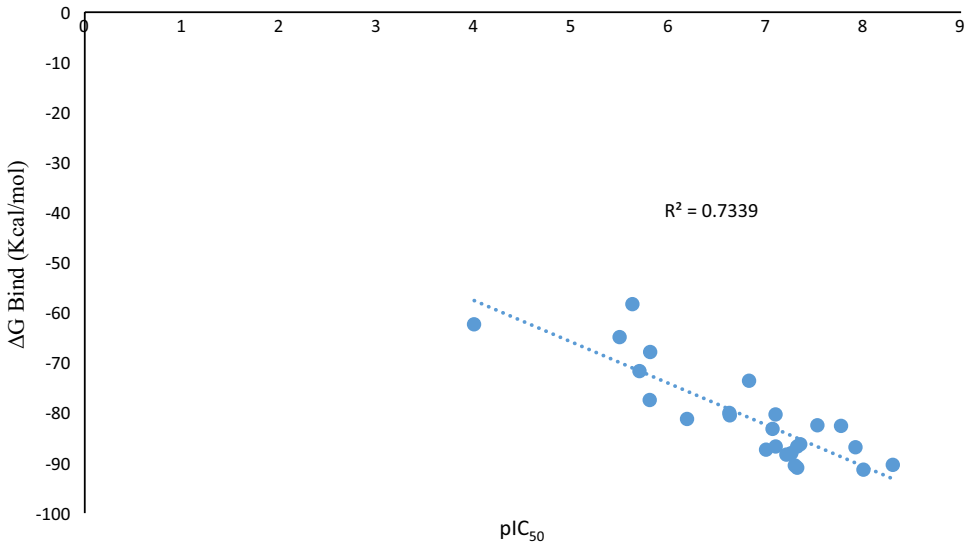

Fig. 2 Binding free energy versus pIC_{50} correlation graph with correlation value R^2

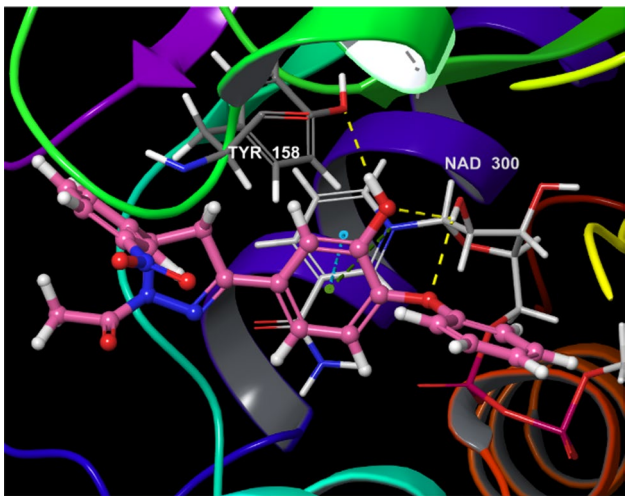

Fig. 3 Induced fit docked pose of PYN-8 on 3FNE

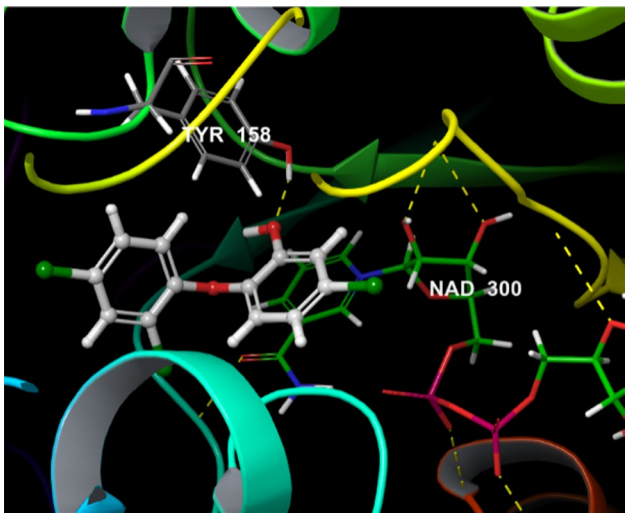

Fig. 4 Induced fit docked pose of triclosan on 3FNE

NAD 300 was also observed. The induced fit docking score of synthesized PYN-8 (−541.09) was better than triclosan (−536.48) supporting its better activity. The interactions are shown in Figs. 3 and 4.

Water map analysis

To understand the better activity of meta-nitro-substituted derivative (PYN-8) compared to other analogues, a water map analysis was performed. Water map shows the hydration sites in a protein along with their thermodynamic properties. Based on the disorderliness of the water molecules in the hydration sites, it can be assessed if a hydration site has to be displaced or eschewed [17]. It was observed that molecule PYN-8 displaced a hydration site with site number 68 as shown in Fig. 5. This hydration site has an enthalpy (ΔH) of 2.24 kcal/mol, entropy ($-T\Delta S$) 1.61 kcal/mol and Gibbs free energy (ΔG) 3.85 kcal/mol. These values indicate that it is favourable to displace this hydration site. The meta-nitro group on the phenyl ring of the PYN-8 helps to increase the hydrophobicity of the phenyl ring. The displacement of the unstable water by this hydrophobic group might be the reason for better activity of PYN-8.

Chemistry

The diphenyl ether pyrazoline derivatives were synthesized as depicted in Scheme 1. The synthesis of 1-(3-methoxy-4-phenoxyphenyl)ethanone was done via Chan–Lam coupling. Phenyl boronic acid and acetovanillone were reacted in the presence of copper acetate monohydrate, pyridine in anhydrous dichloromethane with activated molecular sieves

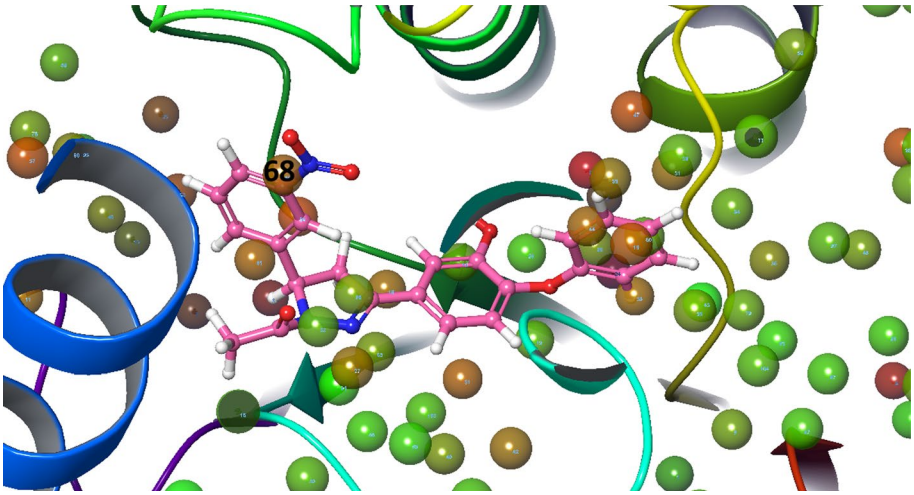

Fig. 5 Water map of 3FNE protein showing PYN-8 displacing water site number 68

Table 3 In vitro MIC values of synthesized derivatives determined against *Mycobacterium tuberculosis* H37Rv strain in two different media

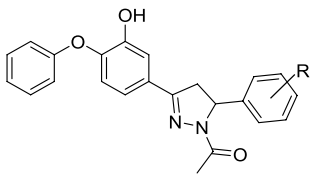

Compound code	R group	(7H9/ADC/Tw) MIC		(GAST-Fe) MIC	
		Day 7 (μM)	Day 14 (μM)	Day 7 (μM)	Day 14 (μM)
PYN-1	4-chloro	123	> 246	61	123
PYN-2	4-nitro	240	> 240	120	> 239
PYN-3	4-bromo	28–55	> 222	28	> 222
PYN-4	4-fluoro	128	128	128	128
PYN-5	4-methyl	> 259	> 239	32	32
PYN-6	4-methoxy	31	> 249	31	62
PYN-7	3-chloro	61	61	61	61
PYN-8	3-nitro	3	4–7	15	15
PYN-9	3-bromo	111–222	111–222	111	111
PYN-10	3-fluoro	64	64	64	64
PYN-11	3-methyl	259	259	129	259
Triclosan	–	21	43	43	43
Isoniazid	–	0.8	1	0.2	0.2–0.4

at room temperature. 1-(3-methoxy-4-phenoxyphenyl)ethanone was then deprotected using BBr_3 in anhydrous dichloromethane at − 78 °C [18]. 1-(3-hydroxy-4-phenoxyphenyl) ethan-1-one thus obtained was reacted with various substituted benzaldehydes using lithium hydroxide monohydrate as catalyst for Claisen–Schmidt condensation in ethanol to give various substituted 1-(3-hydroxy-4-phenoxyphenyl)-3-phenylprop-2-en-1-ones [19].

The 1-(3-hydroxy-4-phenoxyphenyl)-3-phenylprop-2-en-1-ones were then converted to 1-(3-(3-hydroxy-4-phenoxyphenyl)-5-phenyl-4,5-dihydro-1H-pyrazol-1-yl) ethan-1-ones by refluxing them with hydrazine hydrate in acetic acid for a duration of 3 h. The synthesized compounds were purified by crystallization and column chromatography. Structures of all the synthesized final derivatives were confirmed by ^{1}H, ^{13}C NMR and HRMS.

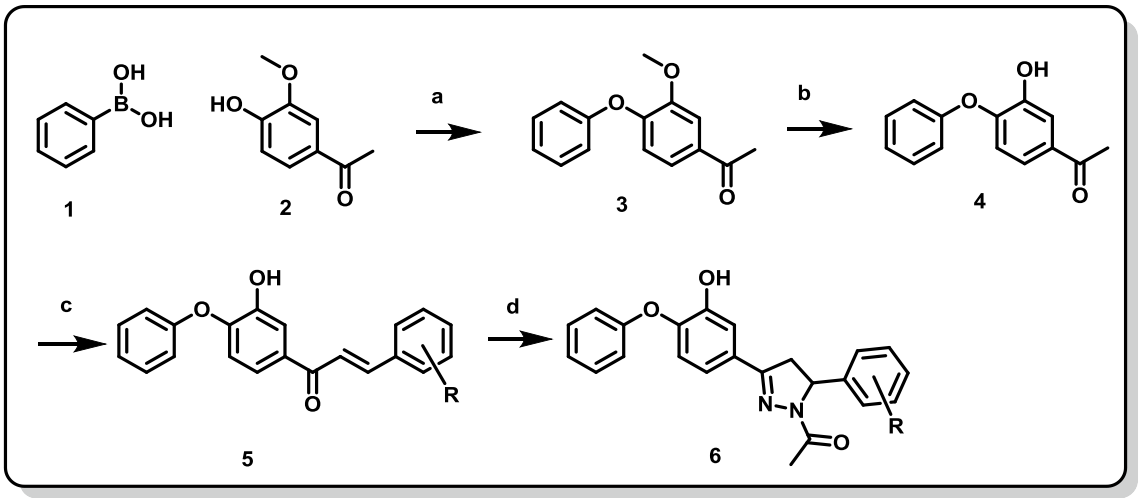

1) Phenyl boronic acid **2)** 3-hydroxy-4-phenoxy **3)** 1-(3-methoxy-4-phenoxyphenyl)ethan-1-one **4)** 1-(3-hydroxy-4-phenoxyphenyl)ethan-1-one **5)** (E)-1-(3-hydroxy-4-phenoxyphenyl)-3-phenylprop-2-en-1-one **6)** 1-(3-(3-hydroxy-4-phenoxyphenyl)-5-phenyl-4,5-dihydro-1H-pyrazol-1-yl)ethan-1-one acetophenone **a)** Copper acetate monohydrate, Pyridine, anhydrous dichloromethane, 4Å Molecular Sieves **b)** BBr_3, anhydrous dichloromethane, -78°C **c)** Substituted benzaldehydes, $LiOH.H_2O$, Ethanol **d)** Hydrazine hydrate, Glacial acetic acid

Scheme 1 Synthesis of pyrazoline derivatives of diphenyl ethers (PYN series)

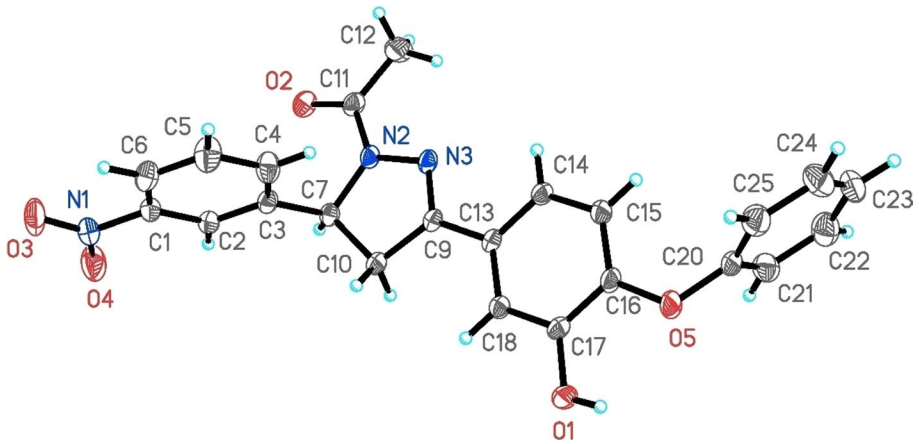

Fig. 6 ORTEP diagram of PYN-8. Displacement ellipsoids are drawn at the 30% probability level

A typical ^{1}H NMR spectrum of 1-(3-(3-hydroxy-4-phenoxyphenyl)-5-phenyl-4,5-dihydro-1H-pyrazol-1-yl)ethan-1-ones showed protons of the pyrazoline moiety at three different positions. The methylene protons in the pyrazoline ring were observed at δ 3.01–3.11 ppm and δ 3.65–3.73 ppm both with a coupling constant of 17.6–17.8 Hz. The stereogenic proton appeared between δ 5.46 and 5.59 ppm with a coupling constant of 11.8–12.0 Hz. A singlet or a small hump at δ 5.7–5.8 ppm indicated the OH protons. The methyl protons of the acetyl group on the nitrogen of pyrazoline ring were observed at δ 2.3–2.42 ppm as a singlet. The HRMS (ESI/Q-TOF) showed $[M+H]^+$ peaks corresponding to their molecular formula weight.

Further, the structure of compound **PYN-8** was confirmed by single-crystal X-ray diffraction study as shown in Fig. 6.

Antitubercular study

All the synthesized final derivatives (1–11) were screened for their antitubercular activity against *Mycobacterium*

Table 4 Percentage inhibition values of cancer cells and *Mycobacterium bovis* at 10 µM concentration of the compounds

Compound code	% inhibition of cells at 10 µM concentration					
	MCF7	PANC-1	PC-3	SKOV-3	HeLa	*M. bovis*
PYN-1	6.77	4.29	17.29	2.71	4.45	10.15
PYN-2	4.75	5.42	18.10	3.05	4.78	23.00
PYN-3	6.16	5.17	− 2.67	4.12	4.10	− 22.14
PYN-4	4.07	3.20	11.41	4.32	3.31	− 19.60
PYN-5	4.04	1.07	− 9.88	4.79	3.06	11.04
PYN-6	1.65	2.17	12.01	0.97	4.40	38.00
PYN-7	5.15	3.27	0.04	4.50	3.66	− 35.36
PYN-8	4.88	4.06	5.06	4.32	3.52	95.91
PYN-9	4.68	2.69	− 4.23	3.92	3.32	29.55
PYN-10	4.80	2.68	− 4.02	4.92	3.25	32.17
PYN-11	5.65	2.27	0.82	3.67	2.99	− 35.31
Doxorubicin (2 µM)	81.84	60.82	76.52	77.37	47.91	–
Rifampicin	–	–	–	–	–	99.3
Isoniazid	–	–	–	–	–	99.1

tuberculosis, strain H37Rv. They were also tested for their inhibitory effect against *Mycobacterium bovis*. The derivative with meta-nitro substitution PYN-8 showed better activity than the other analogues. Similar trend of activity in both *Mycobacterium tuberculosis* and *Mycobacterium bovis* signifies the activity values. The activity values are reported in Table 3.

Cytotoxicity assay

For the treatment of tuberculosis, it is essential to take antitubercular drugs for a long period of time (at least 6 months). Thus, it is necessary to study cytotoxic effects of the drug candidates. The compounds were therefore evaluated at 10 µM concentration for their cytotoxic effect on MCF-7, PANC-1, PC-3, SKOV-3 and HeLa cell lines. Additionally, they were screened against BD-11 and HEK cell lines where their cytotoxic concentration was greater than 100 µM. Therefore, these studies indicate that these compounds do not have any cytotoxic effect. The cytotoxicity data are shown in Table 4.

Drug likeness properties

In the advanced drug discovery phases, many hits often don't succeed [20]. Therefore, it is vital to evaluate lead likeness and drug likeness of hits obtained after a comprehensive screening of molecules. Lipinski's rule of five was

Table 5 In silico ADME properties as predicted by Qikprop

Compound	Mol MW	HD	HA	QPlogPo/w	QPPCaco	QPlog BB	%Human oral absorption	Rule of five	PSA
PYN-1	406.8	1	4.75	5.291	1605.4	− 0.305	100	1	69.6
PYN-2	417.4	1	5.75	4.084	192.5	− 1.564	91.747	0	114.7
PYN-3	451.3	1	4.75	5.367	1609.9	− 0.293	100	1	70.4
PYN-4	390.4	1	4.75	5.036	1596.5	− 0.358	100	1	69.7
PYN-5	386.4	1	4.75	5.107	1609.4	− 0.484	100	1	70.3
PYN-6	402.4	1	5.5	4.928	1782.8	− 0.5	100	0	78.1
PYN-7	406.8	1	4.75	5.335	1802.7	− 0.254	100	1	69.6
PYN-8	417.4	1	5.75	4.127	217.1	− 1.516	92.936	0	113.1
PYN-9	451.3	1	4.75	5.412	1803.4	− 0.244	100	1	69.6
PYN-10	390.4	1	4.75	5.075	1801.3	− 0.304	100	1	69.9
PYN-11	386.4	1	4.75	5.148	1814.6	− 0.431	100	1	69.8

HD hydrogen bond donor, *HA* hydrogen bond acceptor, *PSA* polar surface area

formulated to ascertain drug likeness of a chemical compound with properties that would probably make it an orally active drug. Molecules which comply with these rules experience lower attrition and failure in clinical trials in the drug discovery process. The probability of reaching the market for such molecules increases because the parameters of this rule were set after observing that most of the orally administered drugs are moderately lipophilic and small molecules [21]. Thus, we also determined the ADME properties of the synthesized compounds in silico, and all the compounds showed desirable ADME profile (Table 5).

Conclusion

A protein crystal structure, **3FNE,** was selected after screening all the available protein X-ray crystal structures from protein data bank. The selection was made after cross-docking and validation study of the protein crystal structures. The molecules were designed using insights from the interaction patterns of known diphenyl ether derivatives. The synthesized compounds were then evaluated for their antitubercular activity against *Mycobacterium tuberculosis* H37Rv strain and *Mycobacterium bovis*. Compound **PYN-8** was found to be most active among the synthesized derivatives with MIC = 4–7 μM in 7H9/ADC/Tw medium and showed a 95.91% inhibition of *Mycobacterium bovis* at 10 μM concentration. All the synthesized compounds were subjected to cytotoxicity evaluation against various cell lines and were found to be noncytotoxic. The ADME properties calculated in silico predicted good pharmacokinetic profile of the synthesized molecules. These analogues can be further developed to improve their InhA inhibitory activity.

Experimental

General chemistry

All chemicals and reagents for synthesis were procured from Sigma-Aldrich (St. Louis, MO, USA) and Spectrochem Pvt. Ltd. (Bengaluru, India). LR-grade solvent was used in the reaction. Distilled solvents were used for column chromatography (CC). Silica gel 60 F254-precoated TLC (thin-layered chromatography) plates were used for monitoring the reactions and visualized in UV chamber. The compounds were purified by CC or recrystallization. Column chromatography was performed on silica gel 60120 (100–200 mesh). Silica gel for CC and TLC plate both was purchased from Merck (Germany). The synthesized compounds were characterized using ^{1}H and ^{13}C NMR and mass spectrometry. ^{1}H- and ^{13}C-NMR spectra were recorded using Bruker Ascend 400 MHz; chemical shift values (δ) are expressed in ppm relative to internal standard, tetramethylsilane (TMS). The mass spectra were recorded on Agilent Technologies 6545 Q-TOF LC/MS.

Synthesis of 1-(3-methoxy-4-phenoxyphenyl) ethan-1-one

1-(3-methoxy-4-phenoxyphenyl)ethan-1-one was synthesized as described in the previously reported procedure [22]. The compound was used without further purification in the next step with a crude yield of 81%.

Synthesis of 1-(3-hydroxy-4-phenoxyphenyl) ethan-1-one

1-(3-hydroxy-4-phenoxyphenyl)ethan-1-one was synthesized from 1-(3-methoxy-4-phenoxyphenyl)ethanone as described in the previously reported procedure [22]. The crude compound was purified using column chromatography using ethyl acetate: hexane (3:7) to give 76% yield.

Synthesis of 1-(3-hydroxy-4-phenoxyphenyl)-3-phenylprop-2-en-1-ones

1-(3-hydroxy-4-phenoxyphenyl)ethan-1-one (0.66 mmol) in EtOH (1 mL) and $LiOH{\cdot}H_2O$ (1.4 mmol) was stirred for 10 min at room temperature. Then, various substituted benzaldehydes (0.79 mmol) were added and stirred at room temperature until complete consumption of the starting materials. A yellow precipitate was usually obtained after completion of the reaction. EtOH was removed under reduced pressure. The residue was diluted with water (5 mL) and neutralized with 2% dilute HCl. It was then extracted with ethyl acetate (10 mL). The organic layer was washed with saturated NaCl solution (5 mL), dried with $MgSO_4$ and concentrated under reduced pressure. It was then re-crystallized from ethanol to afford various phenylprop-2-en-1-ones in 80–89% yield.

General method for the synthesis of substituted 1-(3-(3-hydroxy-4-phenoxyphenyl)-5-phenyl-4,5-dihydro-1H-pyrazol-1-yl)ethan-1-one

1-(3-hydroxy-4-phenoxyphenyl)-3-phenylprop-2-en-1-ones (0.47 mmol) and hydrazine hydrate (1.41 mmol) in glacial acetic acid (2 mL) were refluxed for 2 h. Upon completion of the reaction, the mixture was poured into ice cold water (20 mL). The precipitate was then filtered and washed with cold water (10 mL) and re-crystallized from ethanol to give pure product.

1-(5-(4-chlorophenyl)-3-(3-hydroxy-4-phenoxyphenyl)-4,5-dihydro-1H-pyrazol-1-yl)ethan-1-one (PYN-1) %Yield: 88%, ^{1}H

NMR (400 MHz, Chloroform-*d*) δ 8.16–7.95 (m, 2H), 7.52 (d, *J* = 7.6 Hz, 1H), 7.49–7.37 (m, 2H), 7.32 (t, *J* = 7.7 Hz, 2H), 7.00 (d, *J* = 8.1 Hz, 2H), 6.79 (d, *J* = 8.4 Hz, 1H), 5.77 (s, 1H), 5.59 (dd, *J* = 12.0, 5.0 Hz, 1H), 3.73 (dd, *J* = 17.8, 12.0 Hz, 1H), 3.05 (dd, *J* = 17.8, 5.0 Hz, 1H), 2.36 (s, 3H); ^{13}C NMR (101 MHz, Chloroform-*d*) δ 168.92, 155.89, 153.16, 147.36, 145.98, 140.35, 133.48, 130.11, 129.09, 127.53, 127.13, 124.44, 119.34, 118.74, 117.94, 114.15, 59.46, 42.28, 21.92. HRMS (ESI/Q-TOF) m/z: $[M+H]^+$ Calcd for $C_{23}H_{19}ClN_2O_3^+$ 407.1157; found 407.1148.

1-(3-(3-hydroxy-4-phenoxyphenyl)-5-(4-nitrophenyl)-4,5-dihydro-1H-pyrazol-1-yl)ethan-1-one (PYN-2) %Yield: 91%, ^{1}H NMR (400 MHz, Chloroform-*d*) δ 8.16–8.10 (m, 2H), 7.40 (d, *J* = 2.0 Hz, 1H), 7.37–7.28 (m, 4H), 7.19 (s, 1H), 7.17–7.07 (m, 2H), 7.00 (d, *J* = 8.0 Hz, 2H), 6.79 (d, *J* = 8.5 Hz, 1H), 5.73 (s, 1H), 5.58 (dd, *J* = 12.0, 5.0 Hz, 1H), 3.72 (dd, *J* = 17.7, 12.0 Hz, 1H), 3.03 (dd, *J* = 17.7, 5.0 Hz, 1H), 2.35 (s, 3H); ^{13}C NMR (101 MHz, Chloroform-*d*) δ 155.76, 153.07, 148.82, 147.44, 147.37, 146.24, 130.14, 127.09, 126.70, 124.55, 124.34, 119.38, 118.83, 117.85, 114.15, 59.53, 42.12, 21.84, 1.02. HRMS (ESI/Q-TOF) m/z: $[M+H]^+$ Calcd for $C_{23}H_{19}N_3O_5^+$ 418.1397; found 418.1391.

1-(5-(4-bromophenyl)-3-(3-hydroxy-4-phenoxyphenyl)-4,5-dihydro-1H-pyrazol-1-yl)ethan-1-one (PYN-3) %Yield: 87%, ^{1}H NMR (400 MHz, Chloroform-*d*) δ 7.42–7.35 (m, 3H), 7.32 (t, *J* = 7.8 Hz, 2H), 7.11 (t, *J* = 9.3 Hz, 2H), 7.04 (d, *J* = 8.0 Hz, 2H), 6.99 (d, *J* = 8.0 Hz, 2H), 6.79 (d, *J* = 8.5 Hz, 1H), 5.73 (s, 1H), 5.46 (dd, *J* = 12.5, 4.5 Hz, 1H), 3.65 (dd, *J* = 17.7, 11.9 Hz, 1H), 3.01 (dd, *J* = 17.3, 4.7 Hz, 1H), 2.33 (s, 3H); ^{13}C NMR (101 MHz, Chloroform-*d*) δ 168.94, 155.91, 153.20, 147.39, 146.00, 140.85, 132.03, 130.09, 127.49, 127.46, 124.41, 121.58, 119.33, 118.73, 117.98, 114.18, 59.52, 42.23, 21.90. HRMS (ESI/Q-TOF) m/z: $[M+H]^+$ Calcd for $C_{23}H_{19}BrN_2O_3^+$ 451.0652; found 451.0636.

1-(5-(4-fluorophenyl)-3-(3-hydroxy-4-phenoxyphenyl)-4,5-dihydro-1H-pyrazol-1-yl)ethan-1-one (PYN-4) %Yield: 85%, ^{1}H NMR (400 MHz, Chloroform-*d*) δ 7.48 (d, *J* = 2.1 Hz, 1H), 7.43–7.34 (m, 2H), 7.25–7.14 (m, 4H), 7.06 (dd, *J* = 7.7, 1.5 Hz, 2H), 7.04–6.96 (m, 2H), 6.86 (d, *J* = 8.5 Hz, 1H), 5.77 (s, 1H), 5.56 (dd, *J* = 11.8, 4.6 Hz, 1H), 3.72 (dd, *J* = 17.6, 11.8 Hz, 1H), 3.10 (dd, *J* = 17.7, 4.6 Hz, 1H), 2.40 (s, 3H); ^{13}C NMR (101 MHz, Chloroform-*d*) δ 167.88, 154.89, 152.16, 146.34, 144.91, 129.08, 126.59, 126.43, 126.35, 123.39, 118.30, 117.70, 116.94, 114.86, 114.64, 113.13, 58.36, 41.34, 20.92, − 1.02. HRMS (ESI/Q-TOF) m/z: $[M+H]^+$ Calcd for $C_{23}H_{19}FN_2O_3^+$ 391.1452; found 391.1439.

1-(3-(3-hydroxy-4-phenoxyphenyl)-5-(p-tolyl)-4,5-dihydro-1H-pyrazol-1-yl)ethan-1-one (PYN-5) %Yield: 84%, ^{1}H NMR (400 MHz, Chloroform-*d*) δ 7.47 (d, *J* = 2.0 Hz, 1H), 7.43–7.34 (m, 2H), 7.22–7.13 (m, 2H), 7.06 (d, *J* = 7.7 Hz, 2H), 6.86 (d, *J* = 8.4 Hz, 1H), 5.55 (dd, *J* = 11.8, 4.5 Hz, 1H), 3.69 (dd, *J* = 17.6, 11.8 Hz, 1H), 3.11 (dd, *J* = 17.6, 4.5 Hz, 1H), 2.40 (s, 3H), 2.30 (s, 3H); ^{13}C NMR (101 MHz, Chloroform-*d*) δ 167.02, 154.20, 151.54, 145.61, 143.96, 137.05, 135.47, 128.16, 127.67, 125.94, 123.68, 122.35, 117.38, 116.74, 116.30, 112.41, 57.95, 40.55, 20.06, 19.22. HRMS (ESI/Q-TOF) m/z: $[M+H]^+$ Calcd for $C_{24}H_{22}N_2O_3^+$ 387.1703; found 387.1701.

1-(3-(3-hydroxy-4-phenoxyphenyl)-5-(4-methoxyphenyl)-4,5-dihydro-1H-pyrazol-1-yl)ethan-1-one (PYN-6) %Yield: 87%, ^{1}H NMR (400 MHz, Chloroform-*d*) δ 7.48 (d, *J* = 2.0 Hz, 1H), 7.43–7.34 (m, 2H), 7.22–7.12 (m, 4H), 7.10–7.02 (m, 2H), 6.85 (t, *J* = 8.1 Hz, 3H), 5.82 (s, 1H), 5.54 (dd, *J* = 11.7, 4.5 Hz, 1H), 3.77 (s, 3H), 3.68 (dd, *J* = 17.6, 11.7 Hz, 1H), 3.11 (dd, *J* = 17.6, 4.5 Hz, 1H), 2.39 (s, 3H); ^{13}C NMR (101 MHz, Chloroform-*d*) δ 168.87, 159.04, 156.04, 153.35, 147.44, 145.82, 134.09, 130.06, 127.85, 126.96, 124.29, 119.28, 118.64, 118.11, 114.24, 59.52, 55.29, 42.34, 21.97. HRMS (ESI/Q-TOF) m/z: $[M+H]^+$ Calcd for $C_{24}H_{22}N_2O_4^+$ 403.1652; found 403.1641.

1-(5-(3-chlorophenyl)-3-(3-hydroxy-4-phenoxyphenyl)-4,5-dihydro-1H-pyrazol-1-yl)ethan-1-one (PYN-7) %Yield: 82%, ^{1}H NMR (400 MHz, Chloroform-*d*) δ 7.47 (d, *J* = 2.0 Hz, 1H), 7.38 (t, *J* = 7.9 Hz, 2H), 7.30–7.03 (m, 8H), 6.86 (d, *J* = 8.5 Hz, 1H), 5.54 (dd, *J* = 11.9, 4.7 Hz, 1H), 3.71 (dd, *J* = 17.9, 11.6 Hz, 1H), 3.09 (dd, *J* = 17.7, 4.7 Hz, 1H), 2.42 (s, 3H); ^{13}C NMR (101 MHz, Chloroform-*d*) δ 168.98, 155.93, 153.20, 147.41, 146.00, 143.81, 134.80, 130.23, 130.09, 127.93, 127.47, 125.73, 124.39, 123.92, 119.35, 118.72, 118.01, 114.21, 59.54, 42.32, 21.91. HRMS (ESI/Q-TOF) m/z: $[M+H]^+$ Calcd for $C_{23}H_{19}ClN_2O_3^+$ 407.1157; found 407.1141.

1-(3-(3-hydroxy-4-phenoxyphenyl)-5-(3-nitrophenyl)-4,5-dihydro-1H-pyrazol-1-yl)ethan-1-one (PYN-8) %Yield: 88%, ^{1}H NMR (400 MHz, Chloroform-*d*) δ 8.09–7.99 (m, 2H), 7.52 (d, *J* = 7.6 Hz, 1H), 7.45 (t, *J* = 7.9 Hz, 1H), 7.40 (d, *J* = 2.0 Hz, 1H), 7.32 (t, *J* = 7.7 Hz, 2H), 7.16–7.08 (m, 2H), 7.00 (d, *J* = 8.1 Hz, 2H), 6.79 (d, *J* = 8.4 Hz, 1H), 5.77 (s, 1H), 5.59 (dd, *J* = 12.0, 5.0 Hz, 1H), 3.73 (dd, *J* = 17.8, 12.0 Hz, 1H), 3.05 (dd, *J* = 17.8, 5.0 Hz, 1H), 2.36 (s, 3H); ^{13}C NMR (101 MHz, Chloroform-*d*) δ 169.16, 155.85, 153.09, 148.71, 147.42, 146.21, 143.84, 132.08, 130.11, 129.97, 127.12, 124.46, 122.81, 120.84, 119.41, 118.77, 117.97, 114.24, 59.44, 42.22, 21.88. HRMS (ESI/Q-TOF) m/z: $[M+H]^+$ Calcd for $C_{23}H_{19}N_3O_5^+$ 418.1397; found 418.1386.

1-(5-(3-bromophenyl)-3-(3-hydroxy-4-phenoxyphenyl)-4,5-dihydro-1H-pyrazol-1-yl)ethan-1-one (PYN-9) %Yield: 79%, ^{1}H NMR (400 MHz, Chloroform-*d*) δ 7.47 (d, *J* = 2.1 Hz, 1H), 7.44–7.32 (m, 4H), 7.24–7.13 (m, 4H), 7.10–7.02 (m, 2H), 6.86 (d, *J* = 8.5 Hz, 1H), 5.53 (dd, *J* = 11.9, 4.7 Hz, 1H), 3.72 (dd, *J* = 17.7, 11.9 Hz, 1H), 3.09 (dd, *J* = 17.7, 4.7 Hz, 1H), 2.42 (s, 3H); ^{13}C NMR (101 MHz, Chloroform-*d*) δ 169.00, 155.93, 153.22, 147.41, 146.02, 144.07, 130.87, 130.52, 130.09, 128.63, 127.45, 124.39, 123.01, 119.36, 118.71, 118.02, 114.23, 59.49, 42.34, 21.91. HRMS (ESI/Q-TOF) m/z: $[M+H]^+$ Calcd for $C_{23}H_{19}BrN_2O_3^+$ 451.0652; found 451.0634.

1-(5-(3-fluorophenyl)-3-(3-hydroxy-4-phenoxyphenyl)-4,5-dihydro-1H-pyrazol-1-yl)ethan-1-one (PYN-10) %Yield: 81%, 1H NMR (400 MHz, Chloroform-d) δ 7.46 (d, J = 2.0 Hz, 1H), 7.38 (t, J = 7.9 Hz, 2H), 7.29 (td, J = 7.6, 5.5 Hz, 1H), 7.22–7.14 (m, 2H), 7.09–6.99 (m, 3H), 6.99–6.88 (m, 2H), 6.86 (d, J = 8.4 Hz, 1H), 5.57 (dd, J = 11.8, 4.6 Hz, 1H), 3.71 (dd, J = 17.7, 11.9 Hz, 1H), 3.09 (dd, J = 17.7, 4.6 Hz, 1H), 2.42 (s, 3H); 13C NMR (101 MHz, Chloroform-d) δ 167.97, 154.95, 152.26, 146.42, 144.98, 129.55, 129.47, 129.05, 126.47, 123.32, 120.26, 120.24, 118.29, 117.66, 117.05, 113.73, 113.52, 113.22, 111.67, 111.45, 58.53, 41.29, 20.86. HRMS (ESI/Q-TOF) m/z: [M + H] + Calcd for $C_{23}H_{19}FN_2O_3$ + 391.1452; found 391.1439.

1-(3-(3-hydroxy-4-phenoxyphenyl)-5-(m-tolyl)-4,5-dihydro-1H-pyrazol-1-yl)ethan-1-one (PYN-11) %Yield: 84%, ^{1}H NMR (400 MHz, Chloroform-*d*) δ 7.48 (d, *J* = 2.0 Hz, 1H), 7.38 (t, *J* = 7.8 Hz, 2H), 7.19 (dd, *J* = 8.6, 5.9, 2.6 Hz, 3H), 7.04 (dd, *J* = 17.6, 6.5 Hz, 5H), 6.86 (d, *J* = 8.4 Hz, 1H), 5.55 (dd, *J* = 11.8, 4.5 Hz, 1H), 4.78 (s, 8H), 3.70 (dd, *J* = 17.6, 11.8 Hz, 1H), 3.11 (dd, *J* = 17.7, 4.6 Hz, 1H), 2.42 (s, 3H), 2.32 (s, 3H); ^{13}C NMR (101 MHz, Chloroform-*d*) δ 168.98, 156.03, 153.47, 147.44, 145.86, 141.79, 138.59, 130.06, 128.82, 128.48, 127.79, 126.17, 124.29, 122.55, 119.31, 118.64, 118.11, 114.27, 60.04, 42.52, 21.94, 21.47. HRMS (ESI/Q-TOF) m/z: $[M+H]^+$ Calcd for $C_{24}H_{22}N_2O_3^+$ 387.1703; found 387.1691.

Antitubercular activity

Antimycobacterial assay

Mycobacterium bovis (BCG) Pasteur is a surrogate model for high-throughput screening of chemical compounds to identify newer antimycobacterial agents [23]. Primary screening of the compounds at 10 µM concentration against *Mycobacterium bovis* was performed in flat-bottomed polystyrene microtiter 96-well sterile plates (Nunc). Test compounds prepared in DMSO were dispensed into triplicate wells before addition of the assay components. 10 µM final concentration of the compounds in the microtiter plate wells was obtained by adding 98 µL of inoculum. Inoculum was an overnight culture with 0.6 optical density diluted with 7H9 broth in 1:1000 ratio. Checks such as DMSO as solvent control, media control (blank) and rifampicin and isoniazid as positive controls to inhibit the growth of *Mycobacterium bovis* in each plate were added for the purpose of better determining the activity of compounds. To prevent evaporation from the wells during assay, sterile distilled water was filled in the peripheral wells. Plates were then incubated at 37 °C and at 80% relative humidity for 4 days. Growth of the bacteria was studied after the incubation period using turbidometry, by measuring the absorbance at 600 nm using a Multi-Mode Reader (PerkinElmer). Percentage growth inhibition was determined against DMSO control. The inhibition of growth of bacteria due to the compounds was calculated as:

$$\text{Percentage Inhibition} = 100 \times \left[\text{OD with compound} - \text{OD of Negative control}\right] / \left[\text{OD of Positive control} - \text{OD of Negative control}\right].$$

M. tuberculosis (H37Rv) inhibition assay

All the final synthesized substituted diphenyl ether derivatives were evaluated for in vitro antitubercular activity against *Mycobacterium tuberculosis* H37Rv strain. Minimum inhibitory concentrations (MIC) were determined in two different media: iron-supplemented GAST (pH 6.6) and in Middlebrook 7H9 broth base supplemented with 0.2% glycerol, 0.4% glucose, 0.5% BSA fraction V, 0.08% NaCl and 0.05% Tween 80. The assay was performed using the serial dilution technique where the *Mycobacterium tuberculosis* inoculum was added to the assay plate containing serial twofold dilutions of the compounds in the medium of choice. A final cell concentration of $1x10^5$ cfu/mL and final compound concentration series in the range of 100–0.78 µg/mL were obtained. Plates were read after completion of week 1 and week 2 of incubation period at 37 °C using inverted enlarging mirror plate reader and graded for growth and no growth. The lowest concentration of compound that completely inhibited growth of the bacterium was reported as MIC [24–26].

Cytotoxicity

Resazurin assay

All cell lines used in this study were purchased from the American Type Culture Collection (ATCC). MCF7,

PANC-1, PC-3, SKOV-3 and HeLa were cultured in Dulbecco's Modified Eagle's Medium (containing 10% FBS in a humidified atmosphere of 5% CO_2 at 37 °C). PC-3 cells were grown in RPMI-1640 medium containing 10% FBS, 1 mM sodium pyruvate 10 mg/mL bovine insulin and non-essential amino acids. The synthesized test compounds were evaluated for their in vitro antiproliferative activity in five different human cancer cell lines by resazurin assay. Cells were seeded in 100-µL aliquots into 96-well microtiter plates at plating densities depending on the duplication time of individual cell lines. Prior to the addition of test compounds, microtiter plates were incubated at 37 °C, 5% CO_2, 95% air, and 100% relative humidity for 24 h. Aliquots of 1 µL of the test compounds were added to the wells in triplicates containing 100 µL of cells, furnishing final drug concentrations. Plates were then incubated further for 48 h. Assay was terminated by adding 50 µL of resazurin solution and then incubating for 60 min at 37 °C. Using a multimode plate reader (Tecan M200) at a wavelength of 560-nm excitation/590 nm, the emission fluorescence intensity was read. The cell growth is directly proportional to the measure of absorbance and is used to calculate the IC_{50} values.

$$\text{Percentage Inhibition} = 100 \times \left[\text{OD with compound} - \text{OD of Negative control}\right] / \left[\text{OD of Positive control} - \text{OD of Negative control}\right].$$

Sulforhodamine B assay

Cytotoxicity of the compounds was also tested on BD-11 and HEK cell lines using sulforhodamine B (SRB) (Sigma-Aldrich, Germany) microculture colorimetric assay. On day zero, cells were seeded in 96-well plates, at appropriate cell densities. They were treated with serial dilutions of the compounds (6.25 to 100 1M) after 24 h. The plates were incubated at 37 °C in a humidified incubator with 5% CO_2 for 96 h. Care was taken to ensure that the final concentration of DMSO does not exceed 0.5%, which was shown to be non-toxic to the cells. Ninety-six hours after drug exposure, percentage of surviving cells was determined in comparison with untreated controls. The cells were fixed with 10% trichloroacetic acid after discarding the supernatant medium from the 96-well plates. The plates were then allowed to stand at 4 °C. Then, the cells were washed in a strip washer four times with water using alternate dispensing and aspiration procedures. 100 µL of 0.05% SRB was incubated at room temperature for about 30 min. After dying, the plates were washed with 1% acetic acid to remove the dye and allowed to air dry overnight. Then, 50 µL of 10 mM Tris base solution (pH-10) was added to each well and absorbance was measured at 520 nm using a 96-well plate reader (Tecan Spectra, Crailsheim, Germany). IC_{50} was calculated using GraphPad Prism software.

Drug design strategy

Data set for cross-docking study

A total of 87 crystal structures of enoyl-acyl carrier protein reductase of *Mycobacterium tuberculosis* available in RCSB protein data bank were selected for the present study. However, only the crystal structures containing co-crystallized inhibitors similar to triclosan were selected for the study. Of the numerous chains of InhA, only the A-chain was considered for the comparative study of the crystal structures. Out of 15 selected crystal structures, 4 were not considered appropriate for the study because they either had a missing inhibitor ligand in the A-chain or had missing coordinates for the substrate binding loop.

Protein preparation

Selected 11 protein crystal structures were prepared using protein preparation module of Schrodinger. Bond orders of the protein structure were assigned, and hydrogens were added. The hydroxyl, asparagine, glutamine and histidine states were optimized using ProtAssign. The complex was subjected to restrained minimization using OPLS_2005 force field, which was terminated when the root-mean-square deviation of the heavy atoms relative to their initial location reached a maximum value of 0.3 Å.

The inhibitor ligands from respective crystal structures were extracted out and were aligned using flexible shape-based alignment in the flexible ligand alignment module as shown in Fig. 7. The prepared protein structures were aligned on the protein PDB entry code 2X23 [27] according to the

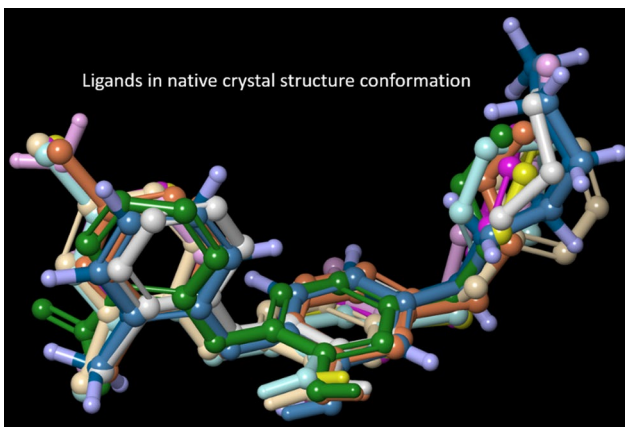

Fig. 7 All the extracted ligands aligned using flexible ligand alignment

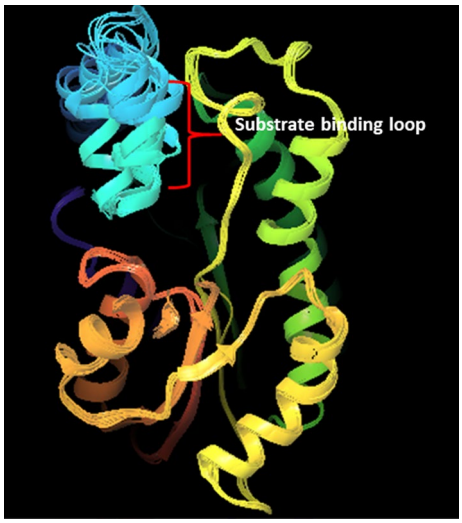

Fig. 8 All 11 crystal structures aligned over 2X23 crystal structure

protein back bone using protein structure alignment as shown in Fig. 8. In order to test the significance of water molecules in the study, another set of protein structures were created by removing all the water molecules from the crystal structures.

Receptor grid generation

Receptor grid was then generated on the chain-A of all the prepared protein structures using glide grid generation with centre of the grid as centroid of the co-crystallized ligand.

Docking

Docking was performed using glide dock on each of the protein crystal structures using all the extracted ligands. The docking was performed in extra precision (XP) mode. Every ligand was docked on all the 11 protein crystal structures.

RMSD calculation

The aligned ligands were chosen individually and superpositioned over their docked poses in different protein structures. Root-mean-square deviations (RMSD) of all the docked poses on proteins containing crystal waters and the ones without the crystal water were then determined with respect to the aligned ligand structures.

Data set for correlation study

Twenty-five diphenyl ether derivatives collected from the literature [28] were used for this correlation study. The molecules had wide variation in their range of biological activity. The IC_{50} values were converted to $-\log IC_{50}$ (pIC_{50}).

Molecular docking

All the 25 inhibitors were docked on protein 3FNE which was prepared by using protein preparation wizard module keeping all the default settings and by removing explicitly all the water molecules from the crystal structure. The selected molecules were drawn using build panel in Maestro, Schrödinger. Bond orders of all the structures were corrected, and structures were energy minimized using LigPrep, Schrödinger. Grid was generated by using centroid of the co-crystallized ligand in the protein–ligand complex crystal as centre. Extra precision (XP) mode (Glide, Schrödinger) was applied for analysing the binding modes of the inhibitors.

Prime MM/GBSA calculations

The MM/GBSA binding free energy was calculated (Prime, Schrödinger) using the receptor ligand complex obtained from molecular docking done in extra precision (XP) mode. VSGB2.0 solvation model and OPLS_2005 force field were used for the simulation.

Induced fit docking

The receptor protein and the ligands were prepared as per the protocol mentioned above. Triclosan and PYN-8 were docked into the active site of 3FNE using the induced fit docking protocol (IFD) (Glide, Schrödinger) [29]. First, the van der Waals radii of protein and ligand atoms are scaled down by a factor of 0.5, and ligands are then docked into the fixed receptor using the Glide SP docking protocol. Then, optimal orientation of the side chains of the binding site residues is predicted by Prime. Finally, the optimized binding site was used for re-docking of the ligand and poses were scored with Glide XP. Following IFD, twenty top-scoring poses were obtained.

Water map

Water map (WaterMap, Schrödinger) was generated using the protein 3FNE after preparation of the protein using protein preparation wizard (Epik, Schrödinger) [30]. The calculation was run for 9 ns (300 K, 1 atm) which is a three-step process. It involves running a molecular dynamics simulation of protein–ligand complex with explicit water molecules. Clustering algorithm then locates the hydration sites, and finally, thermodynamic properties of the waters are calculated.

X-ray diffraction

X-ray data of compound PYN-8 were collected at room temperature using a Bruker Smart Apex CCD diffractometer with graphite monochromated MoKα radiation ($\lambda = 0.71073$ Å) with ω-scan method [31]. Preliminary lattice parameters and orientation matrices were obtained from four sets of frames.

Integration and scaling of intensity data were accomplished using SAINT program [31]. The structure was solved by direct methods using SHELXS [32], and refinement was carried out by full-matrix least-squares technique using SHELXL [32]. Anisotropic displacement parameters were included for all non-hydrogen atoms. Oxygen bound hydrogen atoms were located in different Fourier maps, and their positions and isotropic displacement parameters were refined. All hydrogen atoms were positioned geometrically and treated as riding on their parent carbon atoms [C–H = 0.93–0.97 Å and $U_{iso}(H) = 1.2\ U_{eq}(C)$ for other hydrogen atoms]. All attempts to model a disordered ethylacetate solvent (used for crystallization) failed. Therefore, the solvent contributions have been removed using the SQUEEZE procedure in PLATON [33]. SQUEEZE calculated a void volume of approximately 334 $Å^3$ occupied by 73 electrons per unit cell.

Crystal data for PYN-8: C23H19N3O5 ($M = 417.41$ g/mol): triclinic, space group P-1 (no. 2), $a = 11.2865(7)$ Å, $b = 11.4236(7)$ Å, $c = 11.9381(7)$ Å, $\alpha = 115.8430(10)°$, $\beta = 93.3520(10)°$, $\gamma = 111.2500(10)°$, $V = 1247.36(13)$ $Å^3$, $Z = 2$, $T = 294.15$ K, μ(MoKα) = 0.080 mm-1, Dcalc = 1.111 g/cm^3, 15426 reflections measured ($3.924° \le 2\Theta \le 56.71°$), 6041 unique ($R_{int} = 0.0259$, $R_{sigma} = 0.0341$) which were used in all calculations. The final R_1 was 0.0573 ($I > 2\sigma(I)$) and *wR2* was 0.1671 (all data). CCDC 1883097 contains supplementary crystallographic data for the structure. These data can be obtained free of charge at www.ccdc.cam.ac.uk/conts/retrieving.html [or from the Cambridge Crystallographic Data Centre (CCDC), 12 Union Road, Cambridge CB2 1EZ, UK; fax: +44(0) 1223 336 033; email: deposit@ccdc.cam.ac.uk].

Acknowledgements The authors are thankful to Manipal Academy of Higher Education and Manipal College of Pharmaceutical Sciences for providing necessary supports and facilities to carry out the present research work. Authors are thankful to D'IICT and National Mol Bank (NMB) facility of CSIR-IICT, Hyderabad, India, for the help in biological evaluation of compounds. Authors also thank Manipal-Schrödinger Centre for molecular simulations. This work was funded in part by the Intramural Research Program of the NIH, NIAID.

Compliance with ethical standards

Conflict of interest The authors confirm that this article content has no conflict of interest.

References

1. WHO (2018) Tuberculosis (TB). WHO, Geneva
2. World Health Organization (2018) BCG vaccine: WHO position paper, February 2018 – Recommendations. Vaccine 73–96. https://doi.org/10.1016/j.vaccine.2018.03.009
3. WHO (2017) Guidelines for treatment of drug-susceptible tuberculosis and patient care. WHO, Geneva
4. Rožman K, Sosič I, Fernandez R, Young RJ, Mendoza A, Gobec S, Encinas L (2017) A new 'golden age' for the antitubercular target InhA. Drug Discov Today 22(3):492–502
5. Forrellad MA, Klepp LI, Gioffré A et al (2013) Virulence factors of the *Mycobacterium tuberculosis* complex. Virulence. https://doi.org/10.4161/viru.22329
6. Zhang Y, Heym B, Allen B et al (1992) The catalase-peroxidase gene and isoniazid resistance of *Mycobacterium tuberculosis*. Nature. https://doi.org/10.1038/358591a0
7. Narang A, Giri A, Gupta S et al (2017) Contribution of putative efflux pump genes to isoniazid resistance in clinical isolates of *Mycobacterium tuberculosis*. Int J Mycobacteriol 6:177. https://doi.org/10.4103/ijmy.ijmy_26_17
8. McMurry LM, Oethinger M, Levy SB (1998) Triclosan targets lipid synthesis. Nature 394:531–532
9. Parikh SL, Xiao G, Tonge PJ (2000) Inhibition of InhA, the enoyl reductase from *Mycobacterium tuberculosis*, by triclosan and isoniazid. Biochemistry 39:7645–7650. https://doi.org/10.1021/bi0008940
10. Sullivan TJ, Truglio JJ, Boyne ME et al (2006) High affinity InhA inhibitors with activity against drug-resistant strains of *Mycobacterium tuberculosis*. ACS Chem Biol. https://doi.org/10.1021/cb0500042
11. Pan P, Knudson SE, Bommineni GR et al (2014) Time-dependent diaryl ether inhibitors of InhA: structure-activity relationship studies of enzyme inhibition, antibacterial activity, and in vivo efficacy. ChemMedChem. https://doi.org/10.1002/cmdc.201300429
12. am Ende CW, Knudson SE, Liu N et al (2008) Synthesis and in vitro antimycobacterial activity of B-ring modified diaryl ether InhA inhibitors. Bioorganic Med Chem Lett 18:3029–3033. https://doi.org/10.1016/j.bmcl.2008.04.038
13. Luckner SR, Liu N, Am Ende CW et al (2010) A slow, tight binding inhibitor of InhA, the enoyl-acyl carrier protein reductase from *Mycobacterium tuberculosis*. J Biol Chem. https://doi.org/10.1074/jbc.M109.090373
14. Stewart MJ, Parikh S, Xiao G et al (1999) Structural basis and mechanism of enoyl reductase inhibition by triclosan. J Mol Biol. https://doi.org/10.1006/jmbi.1999.2907
15. Freundlich JS, Wang F, Vilchèze C et al (2009) Triclosan derivatives: towards potent inhibitors of drug-sensitive and drug-resistant *Mycobacterium tuberculosis*. ChemMedChem 4:241–248. https://doi.org/10.1002/cmdc.200800261
16. Chollet A, Maveyraud L, Lherbet C, Bernardes-Génisson V (2018) An overview on crystal structures of InhA protein: apo-form, in complex with its natural ligands and inhibitors. Eur J Med Chem 146:318–343. https://doi.org/10.1016/j.ejmech.2018.01.047
17. Cappel D, Sherman W, Beuming T (2017) Calculating water thermodynamics in the binding site of proteins—applications of WaterMap to drug discovery. Curr Top Med Chem. https://doi.org/10.2174/1568026617666170414141452
18. Cheraïti N, Brik ME (1999) Synthesis of a new triprotonated ligand and selective O-demethylation of methyl aryl ether by boron tribromide. Tetrahedron Lett 40:4327–4330. https://doi.org/10.1016/S0040-4039(99)00786-8
19. Bhagat S, Sharma R, Sawant DM, Sharma L, Chakraborti AK (2006) LiOH · H_2O as a novel dual activation catalyst for highly

efficient and easy synthesis of 1, 3-diaryl-2-propenones by Claisen—Schmidt condensation under mild conditions. J Mol Catal A: Chem 244(1–2):20–24. https://doi.org/10.1016/j.molcata.2005.08.039
20. Wei E, Liu B, Lin S, Liang F (2014) Multicomponent reaction of chalcones, malononitrile and DMF leading to γ-ketoamides. Org Biomol Chem 12:6389–6392. https://doi.org/10.1039/c4ob00971a
21. Lipinski CA (2004) Lead- and drug-like compounds: the rule-of-five revolution. Drug Discov Today Technol 1(4):337–341
22. Kar SS, Bhat VG, Shenoy VP et al (2018) Design, synthesis and evaluation of novel diphenyl ether derivatives against drug susceptible and resistant strains of *Mycobacterium tuberculosis*. Chem Biol Drug Des. https://doi.org/10.1111/cbdd.13379
23. Khan A, Sarkar D (2008) A simple whole cell based high throughput screening protocol using *Mycobacterium bovis* BCG for inhibitors against dormant and active tubercle bacilli. J Microbiol Methods. https://doi.org/10.1016/j.mimet.2008.01.015
24. Barot KP, Jain SV, Gupta N et al (2014) Design, synthesis and docking studies of some novel (R)-2-(4′- chlorophenyl)-3-(4′-nitrophenyl)-1,2,3,5-tetrahydrobenzo[4,5] imidazo [1,2-c]pyrimidin-4-ol derivatives as antitubercular agents. Eur J Med Chem 83:245–255. https://doi.org/10.1016/j.ejmech.2014.06.019
25. Kaniga K, Cirillo DM, Hoffner S et al (2016) A multilaboratory, multicountry study to determine MIC quality control ranges for phenotypic drug susceptibility testing of selected First-Line Antituberculosis Drugs, Second-Line Injectables, Fluoroquinolones, Clofazimine, and Linezolid. J Clin Microbiol. https://doi.org/10.1128/JCM.01138-16
26. Candice SDM, Feng TS, Van Der Westhuyzen R et al (2015) Aminopyrazolo[1,5-a]pyrimidines as potential inhibitors of *Mycobacterium tuberculosis*: structure activity relationships and ADME characterization. Bioorganic Med Chem 23:7240–7250. https://doi.org/10.1016/j.bmc.2015.10.021
27. Kumar V, Sobhia ME (2014) Insights into the bonding pattern for characterizing the open and closed state of the substrate-binding loop in *Mycobacterium tuberculosis* InhA. Future Med Chem. https://doi.org/10.4155/fmc.14.27
28. Pan P, Tonge J, Tonge P (2012) Targeting InhA, the FASII enoyl-ACP reductase: SAR studies on novel inhibitor scaffolds. Curr Top Med Chem 12:672–693. https://doi.org/10.2174/156802612799984535
29. Sherman W, Day T, Jacobson MP et al (2006) Novel procedure for modeling ligand/receptor induced fit effects. J Med Chem 49:534–553. https://doi.org/10.1021/jm050540c
30. Robinson D, Bertrand T, Carry JC et al (2016) Differential water thermodynamics determine PI3 K-beta/delta selectivity for solvent-exposed ligand modifications. J Chem Inf Model 56:886–894. https://doi.org/10.1021/acs.jcim.5b00641
31. Solutions BAX BRUKER ADVANCED X-RAY SOLUTIONS SMART APEX User's Manual, https://www.ndsu.edu/chemistry/files/mcl/smart5_UserManual.pdf
32. Sheldrick GM (2015) Crystal structure refinement with *SHELXL*. Acta Crystallogr Sect C 71:3–8. https://doi.org/10.1107/S2053229614024218
33. Spek AL (2015) PLATON SQUEEZE: a tool for the calculation of the disordered solvent contribution to the calculated structure factors. Acta Crystallogr Sect C Struct Chem. https://doi.org/10.1107/S2053229614024929

Affiliations

Ashutosh Prasad Tiwari[1] · B. Sridhar[2] · Helena I. Boshoff[3] · Kriti Arora[3] · G. Gautham Shenoy[1] · K. E. Vandana[4] · G. Varadaraj Bhat[1]

✉ G. Varadaraj Bhat
varad.g@manipal.edu

[1] Manipal College of Pharmaceutical Sciences, Manipal Academy of Higher Education, Manipal 576104, India

[2] X-ray Crystallography Division, CSIR – Indian Institute of Chemical Technology, Hyderabad 500607, India

[3] Tuberculosis Research Section, Laboratory of Clinical Immunology and Microbiology, National Institute of Allergy and Infectious Diseases, National Institutes of Health, Bethesda, MD 20892, USA

[4] Department of Microbiology, Kasturba Medical College, Manipal Academy of Higher Education, Manipal 576104, India